Single-Satellite Doppler Localization with Law of Cosines (LOC)[1]

Kar-Ming Cheung, Charles Lee
Jet Propulsion Laboratory.
California Institute of Technology
4800 Oak Grove Dr.
Pasadena, CA 91109
Kar-Ming.Cheung@jpl.na@jpl.nasa.gov

William Jun, Glenn Lightsey
Georgia Institute of Technology
North Ave NW
Atlanta, GA 30332
williamjun2@gatech.edu

Abstract— **Modern day localization requires multiple satellites in orbits, and relies on ranging capability which may not be available in most proximity flight radios that are used to explore other planetary bodies such as Mars or Moon. The key results of this paper are:**

1. **A novel relative positioning scheme that uses Doppler measurements and the principle of the Law of Cosines (LOC) to localize a user with as few as one orbiter.**
2. **The concept of "pseudo-pseudorange" that embeds the satellite's velocity vector error into the pseudorange expressions of the user and the reference station, thereby allowing the LOC scheme to cancel out or to greatly attenuate the velocity error in the localization calculations.**

In this analysis, the Lunar Relay Satellite (LRS) was used as the orbiter, with the reference station and the user located near the Lunar South Pole. Multiple Doppler measurements by the stationary user and the reference station at different time points from one satellite can be made over the satellite's pass, with the measurements in each time point processed and denoted as from a separate, faux satellite.

The use of the surface constraint assumption was implemented with this scheme; using the knowledge of the altitude of the user as a constraint. Satellite's ephemeris and velocity, and user's and reference station's Doppler measurement errors were modeled as Gaussian variables, and embedded in Monte Carlo simulations of the scheme to investigate its sensitivity with respective to different kinds of errors.

With only two Doppler measurements, LOC exhibited root mean square (RMS) 3D positional errors of about 22 meters in Monte Carlo simulations. With an optimal measurement window size and a larger number of measurements, the RMS error improved to under 10 meters. The algorithm was also found to be fairly resilient to satellite velocity error due to the error mitigating effects in the LOC processing of the pseudo-pseudorange data type.

A sensitivity analysis was performed to understand the effects of errors in the surface constraint, showing that overall position error increased linearly with surface constraint error. An analysis was also performed to reveal the relationship between the distance between the user and the reference station; a distance of up to 100 km only lead to an increase of 10 meters in RMS 3D position error.

Ultimately, the LOC scheme provides localization with a minimal navigation infrastructure that relaxes hardware requirements and uses a small number of navigation nodes (as small as one).

TABLE OF CONTENTS

1. INTRODUCTION

The majority of localization schemes for Earth's navigation today use range measurements to perform position fixing. These pseudorange-based localization schemes can achieve down to sub-decimeter accuracy, assuming differential GPS (DGPS) [1]. For the Earth based GPS scheme, each satellite is required to possess dedicated ranging hardware, and there must be a minimum of 24 satellites for 95% coverage [2]. Both of these requirements would be extraneous and ambitious for missions orbiting other planets such as Mars or the Moon.

Current space proximity link radios do not provide ranging functions, but they can measure Doppler. The use of Doppler as a means for localization instead of ranging has been performed in limited aspects, with positioning of emitters with differential Doppler [3] - [5]. However, these methods leverage an active emitter as a user and multiple receivers. This paper introduces a novel relative positioning scheme

978-1-5386-6854-2/19/$31.00 ©2019 IEEE

that localizes a static, passive user (receiver) with a single satellite (emitter). It is based on the principle of the Law of Cosines (LOC) and uses Doppler measurements between the satellite and the user as well as a reference station to infer the user's position relative to the reference station on the surface of a planetary body. The derivation of the LOC scheme is described in Appendix A.

Doppler Measurements

Due to the reliance of the Doppler measurements on the knowledge of the satellite's velocity magnitude and direction, the LOC localization scheme is very sensitive to errors in the satellite's velocity vector. To mitigate this error, the concept and the data type of "pseudo-pseudorange" was introduced that embeds the satellite's velocity error into the pseudorange expressions of the user and the reference station, thereby allowing the LOC scheme to "cancel out" or to greatly attenuate the velocity error in the localization calculations. The details are discussed in Appendix A.

Along with the dependence on satellite velocity, the Doppler measurements rely on the accuracy and consistency of the onboard clock. Innovations have led to small, stable oscillators like the Chip Scale Atomic Clock (CSAC) that could fit onto CubeSat class satellites [6].

Single Satellite Multiple Measurements (SSMM)

To achieve localization with only a single satellite, a technique called Single Satellite Multiple Measurements (SSMM) was used. In this technique, a specified number of Doppler measurements were taken by the user and the reference station over a specified amount of time (measurement window). At each measurement, the line of sight vector from the reference station to the satellite's current position (at the time of measurement) was also stored. The time between each measurement and the final measurement was used along with the precise rotation rate of the planet to rotate each of the line of sight vectors by the amount that the planet had rotated (about the planet's rotation axis). This allows for multiple measurements from one satellite to be used at one time, creating multiple faux satellites that are all directed towards the same static user. The derivation of this technique is described in Appendix C.

Surface Constraint

Another assumption to reduce the number of required measurements was the use of the surface constraint; using the user's altitude (distance from the center of the planet to the user) in the localization algorithm. If a general, regional location of the user is known, along with accurate topographical data of the planet or region, an approximate altitude can be used as a constraint in the solution of the LOC algorithm. The algorithm can also be used without the surface constraint, but many measurements over a long period of time would need to be taken to ensure an accurate initial position fix. Once this has been done however, the calculated altitude can be used as the surface constraint to greatly reduce the number of measurements required (only two for one position fix) and can be updated through dead reckoning. The details are shown in Appendix B.

Applications

The LOC scheme is particularly useful in providing a minimal navigation infrastructure with a small number of navigation nodes (as small as one); for example, users on the Moon and Mars that use current proximity link radios. However, this technique can be used on any planetary body with a reference station in the vicinity of the user and at least one orbiter.

Relaxing the assumption of one satellite, multiple orbiters can be used to increase data diversity. Due to the inherent symmetric ambiguity of Doppler measurements, two (or more) orbiters with different orbit planes would help resolve the ambiguity and mitigate errors in three-dimensions (3D). However, only one satellite was used in this paper's analysis.

Summary of Results

For this single-satellite case under reasonable error assumptions (discussed in the next section), it is shown that at the beginning of the LRS pass and with a wait time of 30 minutes and two measurements, the 3D positioning error is approximately 22 m. With a wait time of 40 minutes with one measurement per minute, the 3D positioning error can be reduced to less than 10 m.

2. LOC Simulation Setup and Results

Simulation Setup

In this paper, the LOC scheme and its performance will be described in the context of the localization of a user on the Lunar South Pole surface with a reference station in its vicinity, and a Lunar Relay Satellite (LRS) in an elliptical frozen orbit with high visibility over the South Pole. The locations of the surface user and the reference station are given in Table 1, and the LRS's orbital elements are given in Table 2 (visualized in Figure 1). The user was 10 km from the reference station.

Table 1: User Locations

User	Location
User (Target)	0° E, 89.6702° S
Reference User (Base)	0° E, 90° S

Table 2: Lunar Relay Satellite (LRS) Orbital Elements on the Moon

a (km)	e	i (deg)	Ω (deg)	w (deg)
6142.4	0.6	57.7	90	180

In this single satellite case, Doppler measurements were sampled at different time points when the LRS was in view with the surface user and the reference station. The user was assumed to be stationary when the samples were taken.

The LOC scheme was simulated using the error assumptions provided in Table 3. The properties of convergence for all Monte Carlo simulations are provided in Table 4

Table 3: Error Standard Deviations

Error	Sigma (σ)
Satellite Ephemeris (3D)	5 m
Satellite Velocity Vector (3D)	1 cm/s
Doppler Measurement	0.005 Hz

Table 4: Convergence and Monte Carlo Properties

Convergence	0.01 cm
Convergence Iteration Limit	25
Monte-Carlo Iterations	10,000
Randomization Algorithm	Gaussian

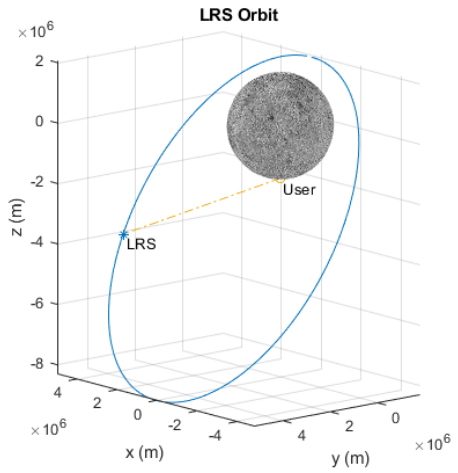

Figure 1: The Lunar Relay Satellite (LRS) Orbit over the Lunar South Pole

All three components of satellite ephemeris and velocity had the respective error standard deviation multiplied by a Gaussian random value (ranging from -1 to 1) added to them; the simulated received Doppler measurement also was summed with the same randomized error.

The satellite ephemeris error was found from general DSN ephemeris error knowledge [7], and the satellite velocity vector error was quoted from the navigation team at the Jet Propulsion Laboratory (JPL)[2]. Finally, the Doppler measurement error was a conservative estimate from Doppler noise values [8].

The assumption of a known surface constraint was used and ideally set to the precise altitude of the user. Along with this, the assumption of SSMM was used along with precise knowledge of the Moon's rotation rate and rotation axis.

Results

A simulation of the LOC algorithm with a moving window of 30 minutes with two measurements (once at the beginning of the window and once at the end) was executed over the entire LRS pass. The converged location was compared to the actual location of the user and an error vector was derived. The magnitude of this error vector, or the 3D position error, and the number of iterations for convergence is shown in Figure 2.

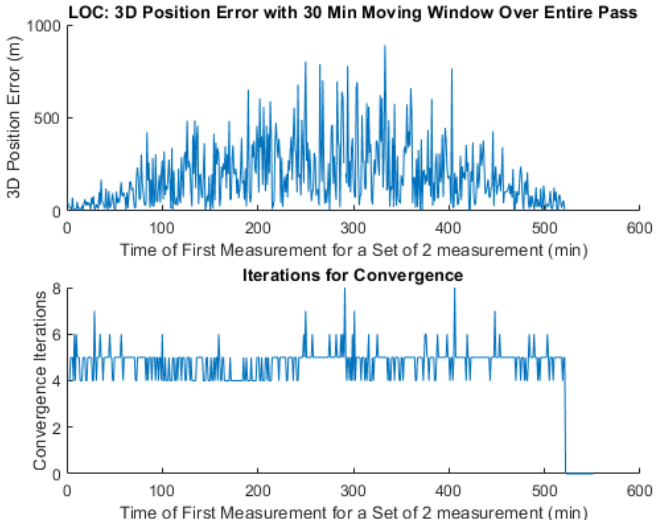

Figure 2: Two Doppler Measurements in a 30-Minute Moving Window over the Entire LRS Pass

The greatest accuracy occurred at the beginning of the pass (Figure 2). This effect aligns with expectations due to the beginning of the pass being the point when the satellite has the largest range rate and is the farthest from being directly overhead the user (the angle between the satellite's velocity vector and the line of sight vector from user to satellite is farthest from 90 degrees). The 3D position error increased at the center of the LRS pass due to the slowing speed of the satellite at its apoapsis and it being close to directly overhead the user, decreasing the noticeable effects of Doppler shifts.

Running a Monte Carlo simulation only at the beginning of the pass, using error values from Table 3, results in a root mean square (RMS) 3D position error of approximately 22 m (Figure 3). This simulation assumed the same characteristics as before: a moving window of 30 minutes with two measurements (once at the beginning of the window and once at the end), the surface constraint, and SSMM.

Due to the dependence of Doppler measurements (and therefore the LOC scheme) on the accuracy of the satellite's velocity vector, the relationship between the resulting 3D

[2] Private communications with Jeffery Stuart, JPL Navigation Team, 2018.

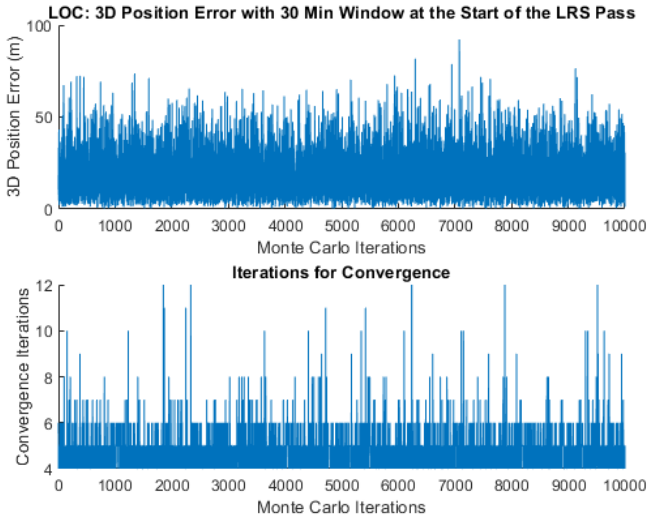

Figure 3: Monte Carlo Analysis of LOC with 2 Measurements and a 30 Minute Window

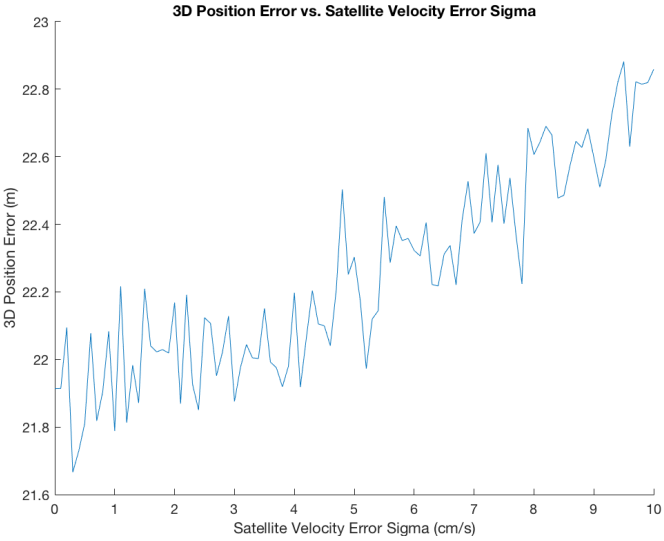

Figure 4: 3D Position Error vs. Satellite Velocity Vector Error for the LOC scheme using two measurements with a 30-minute window at the beginning of the LRS pass

position error and the satellite velocity vector error was evaluated at the beginning of the LRS pass (Figure 4). Each data point was the resulting RMS error from a Monte Carl o simulation following properties from Table 4, only varying the satellite velocity error sigma from 0 to 10 cm/s. The same method of data production was used for Figures 5 – 7.

The LOC scheme was shown to be quite resilient with respect to the LRS's velocity error (Figure 4). Figure 5 displays a larger range of velocity vector error.

The resiliency against increases in satellite velocity vector error was due to the error mitigating effects of the pseudo-pseudorange data type. Again, these expressions embed the satellite velocity vector error into the pseudo-pseudorange equations of both the user and the reference station, and essentially "cancel-out" the error when using relative navigation.

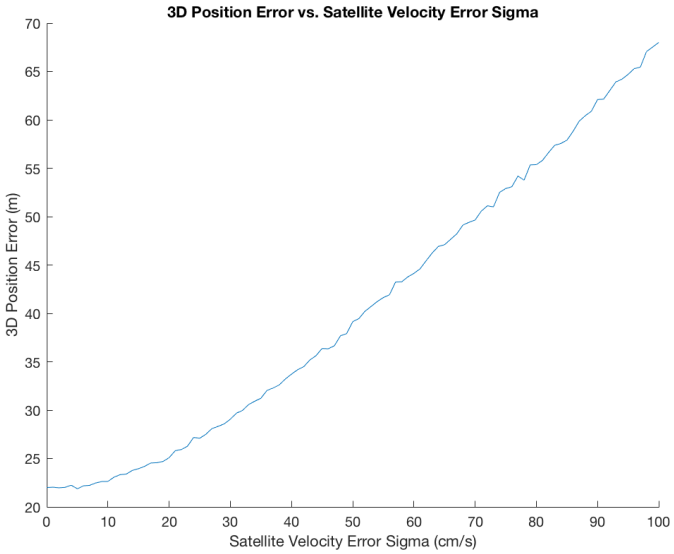

Figure 5: 3D Position Error vs. Satellite Velocity Vector Error for LOC scheme using two measurements with a 30-minute window at the beginning of the LRS pass. With a larger range of satellite velocity error

The overall 3D position error can be further reduced through longer measurement windows and more measurements. Figure 6 displays the relationship between 3D position error and measurement window size with only two measurements (still at the beginning and end of the measurement window).

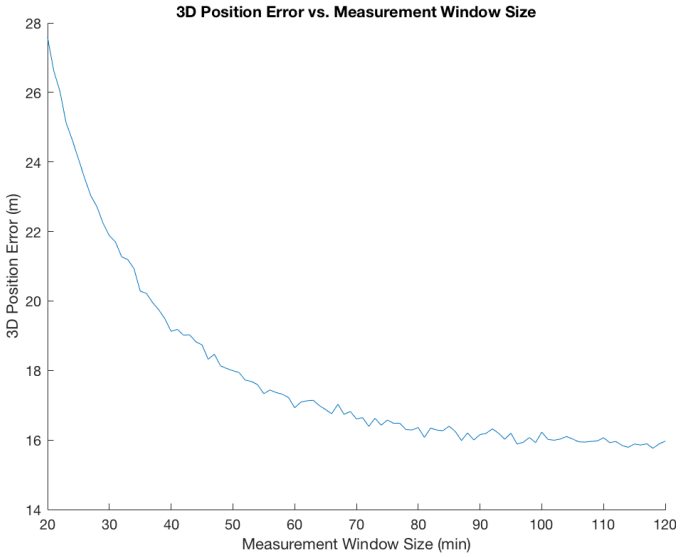

Figure 6: 3D Position Error vs. Measurement Window Size for LOC using two measurements at the beginning of the LRS pass

With only two measurements, accuracy improved with a longer time between measurements, and flattened when the window size reached 120 minutes or more. This was because of the increase of data diversity as the satellite moved through its pass. If more than two measurements are taken however, further improvements can be achieved. Figure 7 demonstrates the 3D position error as a function of the window size with one measurement per minute.

The optimal configuration of was found to be a measurement window of 40 minutes with 1 measurement per minute (40 measurements; Figure 7), resulting in a 3D position error of under 10 meters for the error conditions given in Table 3.

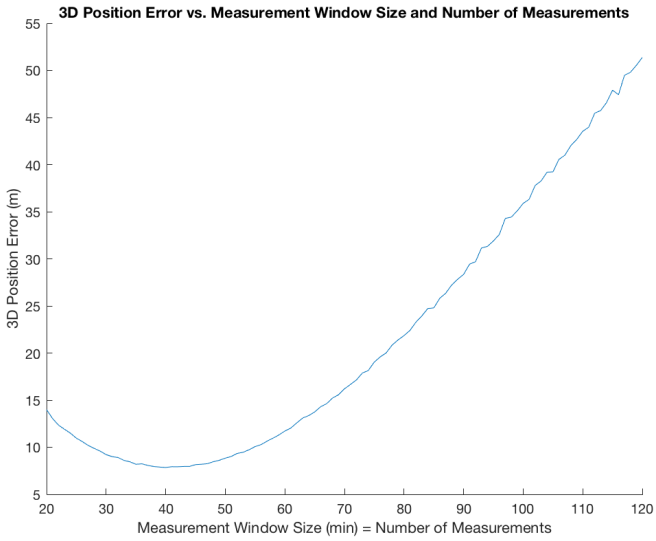

Figure 7: 3D Position Error vs. Measurement Window Size and Number of Measurements per Window for LOC with at the beginning of the LRS pass. There was one measurement per minute in each varying measurement window

A similar configuration of 40 minutes and 38 measurements was confirmed to be the global minimum for the LRS pass with an analysis on variable measurement window size and variable number of measurements (Appendix D).

This configuration was optimized specifically for a measurement window starting at the beginning of the LRS's pass. Figures 5 – 7 are therefore dependent on the satellite's orbit and position during the satellite's pass. If another satellite or another time during the pass was used, this analysis could be performed (even by the user, real time) to solve for the configuration resulting in a local minimum for 3D position error. If passes are predictable, configurations for a global minimum can be solved for and scheduled for frequent position fixes of the user.

3. Surface Constraint Sensitivity Analysis

The assumption of the surface constraint adds previous knowledge of the user's altitude to localization. This can be assumed with an initial knowledge of the user's regional location and with accurate topographical maps of the planetary body. However, if topographical variations exist in the region near the user, the estimate of the user's altitude may contain error. A sensitivity analysis was performed regarding the relationship between the error in known user altitude for the surface constraint and the overall 3D position error. Figure 8 displays the relationship between the error in the surface constraint vs. the overall 3D position error at the optimized measurement configuration calculated before (40-minute window with 38 measurements).

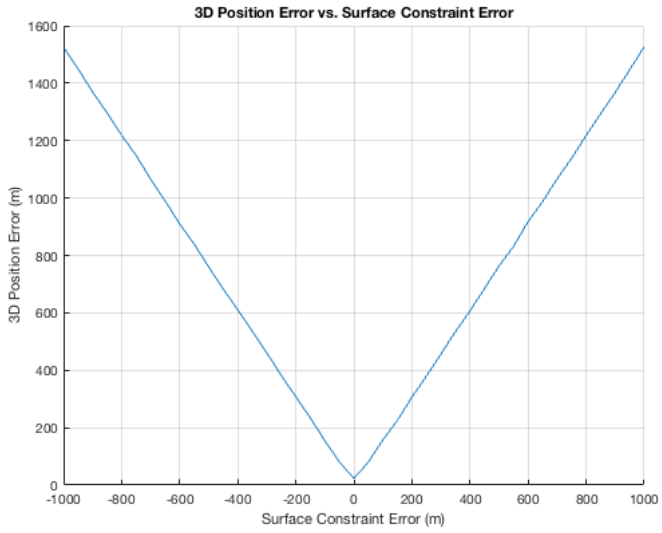

Figure 8: 3D Position Error vs. Surface Constraint Error

In the range of error described in Figure 8, the 3D position error grows linearly with the surface constraint error (Figure 8). This would mean that if the user's altitude was estimated incorrectly by 1 km in the surface constraint, the resulting position fix would also be erroneous by approximately 1.5 km. One solution to this problem would be to initially localize without the surface constraint, then calculate the user's altitude from the position fix. With this newly calculated altitude, the user would then be able to quickly re-localize in the future. This solution could also be used if the user has no previous knowledge of coarse location and therefore cannot infer an altitude from topological maps.

However, due to the lack of the surface constraint, the LOC algorithm was found to require significantly more measurements and a longer measurement window to result in a reliable position fix. The relationship between the measurement window size and the 3D position error for the LOC without the surface constraint is shown in Figure 9.

As shown in Figure 9, a much greater number of measurements and length of measurement window were required to achieve errors similar to those seen with the optimal measurement configuration. If the user can be static for an extended period of time, 3 hours in this case, a fairly accurate position fix can be calculated without the surface constraint. The altitude of this position fix can then be used as the surface constraint in following solutions, drastically reducing the waiting period in between solutions. Figure 10 demonstrates the LOC without a surface constraint, 180 measurements, and a measurement window size of 195 minutes; the RMS 3D position error was approximately 14 meters. This can be improved further with more measurements and a longer measurement window.

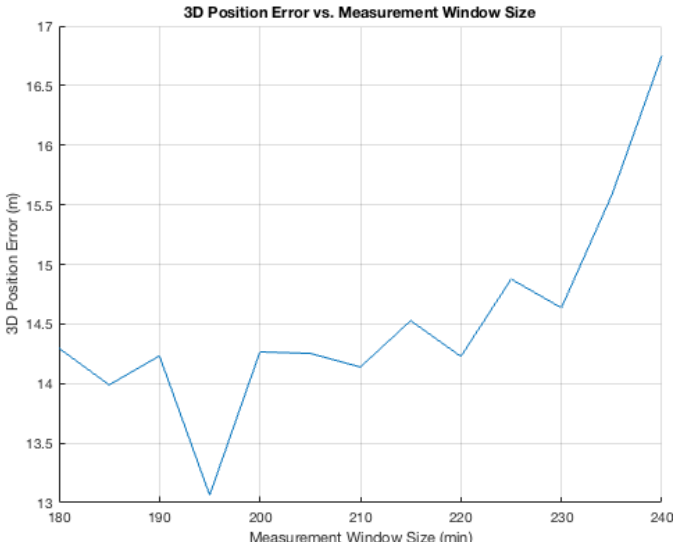

Figure 9: 3D Position Error vs. Measurement Window Size for LOC with 180 measurements per window and no surface constraint

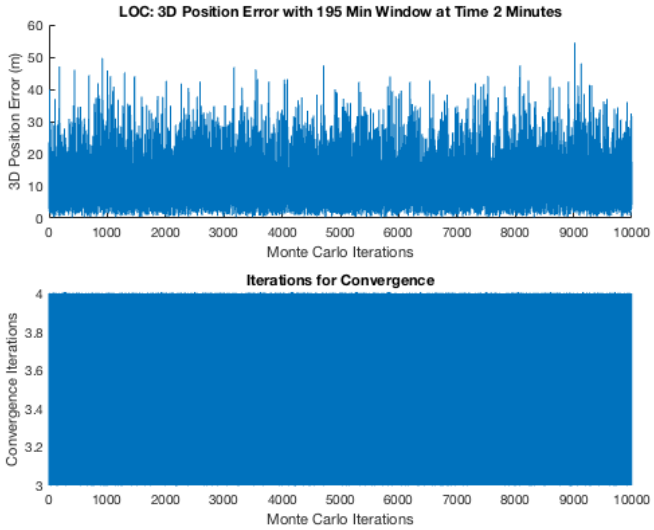

Figure 10: Monte Carlo Simulation of 3D Position Error of LOC with 180 measurements per window, a 195-minute measurement window, and no surface constraint

4. User to Reference Station Distance Analysis

A property that was kept constant throughout this analysis was the distance between the user and the reference station. Because of the importance of this reference station in the implementation of the LOC scheme, the relationship between the relative distance between the user and the reference station was analyzed. This was performed with the optimal configuration that was solved for previously (40 minute measurement window with 38 measurements) and with the surface constraint. The RMS 3D position error vs. the relative location of the user was displayed in Figure 11.

With a distance of up to 100 km away from the reference station, the largest increase in 3D position error was approximately 10 meters (Figure 11). This confirms the resiliency of the LOC algorithm with movement of the user at large distances away from the reference station.

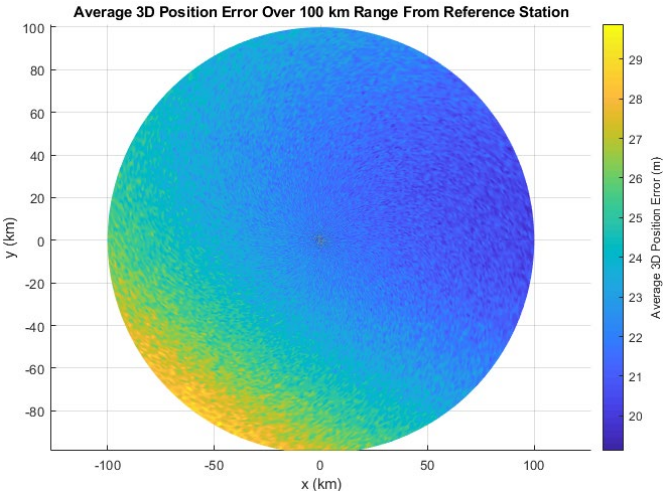

Figure 11: 3D Position Error vs. Relative Location of User with the Reference Station at the center of the circle (0,0)

The error shown in Figure 11 increased with a directional bias towards the lower left direction. This was due to the location of the satellite and the direction of the satellite's velocity at the time of the measurements. The closer the user became to the point exactly nadir from the satellite, the lower the accuracy of the Doppler measurements became, leading to increased 3D position errors.

5. Conclusions and Future Work

With the use of the LOC scheme and some assumptions, precise localization within 25 meters can be accomplished with as few as one satellite. With an optimized configuration for the LRS – dependent on orbital characteristics of the satellite and where it is over its pass – the total 3D position error can be reduced to under 10 meters.

The assumption of the surface constraint added knowledge of user altitude to the system, allowing for less required measurements and improved satellite geometry in most cases. However, if knowledge of planet topography was weak or if the initial, regional location of the user was unknown, LOC without the surface constraint could be used over a large measurement window to localize, using the newly calculated altitude as a surface constraint to lower required measurement window time in future position fixes.

Finally, using the optimal measurement configuration and the surface constraint, the LOC was shown to be resilient to large distances between the user and the reference station, increasing 3D position error by 10 meters with a 100 km user – reference station distance.

Although it still does not reach the sub-meter and sub-decimeter accuracy that ranging based localization techniques can achieve, LOC localizes without the need for ranging hardware, using capabilities that most modern satellites already have. If not used for precise localization,

LOC could be used in emergency situations with any satellite with a radio and any set of users and reference stations.

Related and future works are as follows:

1. New scenarios and possible improvements to LOC will be investigated including multiple reference stations and multiple satellites.

2. Joint Doppler and Ranging (JDR) techniques [9] have been developed, simulated, and analyzed, The JDR scheme[3] enables real-time localization with increased precision, and is more robust with respective to the orbiter - user geometry.

3. The LOC scheme, the JDR scheme and the corresponding concept of pseudo-pseudorange can be promising in improving the current Earth-orbiting navigation satellite systems, which are based on range measurements only. This paper and [9] demonstrate a robust way that an orbiter's velocity can be integrated into the position determination processes. This can result in a) reducing the required number of navigation nodes to calculate a position fix, or b) improving the localization accuracy of existing Earth-orbiting navigation infrastructures.

APPENDICES

A. LOC & PSEUDO-PSEUDORANGE

Measurements of Doppler shift at the user and at the reference station, and the knowledge of the satellite velocity vector and its transmitted frequency can be used to solve for the range rate along the line between the satellite and the user (Equations 1 through 3).

$$Doppler = f_{received} - f_{transmitted} \quad (1)$$

$$f_{received} = f_{transmitted}\left(1 - \frac{RangeRate}{c}\right) \quad (2)$$

$$RangeRate = -c * \frac{Doppler}{f_{transmitted}} \quad (3)$$

This range rate, along with the satellite's velocity vector $\vec{V}_{sat}$, can be used to calculate the angle between the satellite's velocity vector and the line of sight vector from the satellite to the user (Equation 4).

$$cos\theta = -\frac{RangeRate}{\|\vec{V}_{sat}\|} \quad (4)$$

Calculating this angle θ for the user, and similarly the angle ϕ for the reference station, a triangle can be drawn with vertices at the satellite, reference station, and the user at time-point 1 (Figure 12). Note that the velocity vector $\hat{u}_v^1$ and the corresponding angles θ^1 and ϕ^1 are not in general in the same plane defined by C^1, *R,* and *T*.

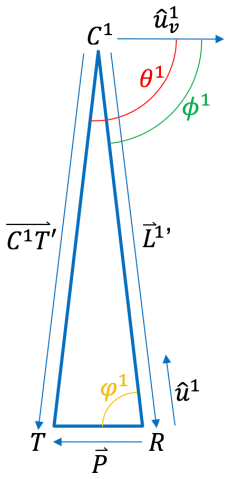

Figure 12: Visual Description of Doppler Localization with Law of Cosines at time-point 1. T is the user, R is the reference station, and C^1 is the satellite. $\hat{u}_v^1$ is the unit vector of the satellite's velocity vector and $\hat{u}^1$is the unit vector from the reference station to the satellite.

The only range information that enters in the LOC calculation is $\|\vec{L}^1\|$, the pseudorange between the satellite C^1 and reference station R whose positions are known, and the altitude of the user on the lunar surface if the surface constraint is used for positioning. From Figure 12, Equations 5, 6, and 7 can be created through the definition of an angle between two vectors. $\|\vec{L}^1\|$ is adjusted with Doppler measurements at the reference station ($\|\vec{L}^{1\prime}\|$) as shown as Equation 5, turning it into a pseudo-pseudorange. Similarly, the unknown pseudorange of the user, which is denoted by $\overrightarrow{C^1T} = \vec{L}^1 + \vec{P}$, is also adjusted as shown in Equation 6.

$$\text{Pseudo-pseudorange } \|\vec{L}^{1\prime}\| = \frac{\vec{L}^1 \cdot \hat{u}_v^1}{cos\phi^1} \quad (5)$$

$$\text{Pseudo-pseudorange } \left\|\overrightarrow{C^1T'}\right\| = \frac{(\vec{L}^1+\vec{P}) \cdot \hat{u}_v^1}{cos\theta^1} \quad (6)$$

$$cos\varphi^1 = \frac{\vec{P} \cdot \hat{u}^1}{\|\vec{P}\|} \quad (7)$$

Now that the equations for the pseudo-pseudoranges of the reference station and user, $\|\vec{L}^{1\prime}\|$ and $\left\|\overrightarrow{C^1T'}\right\|$ respectively, and the angle φ^1 are derived, the Law of Cosines is used to tie the quantities together (Equation 8).

$$\left\|\overrightarrow{C^1T'}\right\|^2 = \|\vec{L}^{1\prime}\|^2 + \|\vec{P}\|^2 - 2\|\vec{L}^{1\prime}\|\|\vec{P}\|cos\varphi^1 \quad (8)$$

Equations 5 – 8 can be converted into a cost function to solve for the vector $\vec{P}$ (Equations 9 - 10).

$$f^1 = \|\vec{L}^{1\prime}\|^2 + \|\vec{P}\|^2 - 2\|\vec{L}^{1\prime}\|\|\vec{P}\|cos\varphi^1 - \left\|\overrightarrow{C^1T'}\right\|^2 \quad (9)$$

[3] Patent application pending.

For the general case of time-point *i*, the cost function can be written in terms of the vector $\vec{P}$ as follows (Equation 10).

$$f^i = \left\|\vec{L}^{i\prime}\right\|^2 + \left\|\vec{P}\right\|^2 - 2\left\|\vec{L}^{i\prime}\right\|\left\|\vec{P}\right\| cos\varphi^i - \left\|\overrightarrow{C^iT'}\right\|^2 \quad (10)$$

As can be seen from Figure 12, errors in the satellite velocity vector will be present in the angles θ^1 and ϕ^1; these angles are used in the pseudo-pseudorange equations 5 and 6. Because the reference station and the user will see approximately the same error in these angles, the effect of the satellite velocity error will be "cancelled out" during the subtraction of these two pseudo-pseudoranges in the cost function (Equation 10).

Finally, the Jacobian of this cost function can be calculated (Equation 11). For $\vec{P} = \begin{bmatrix} x \\ y \\ z \end{bmatrix}$,

$$J^{i1}(x,y,z) = \frac{\partial f^i}{\partial x} \quad (11a)$$

$$J^{i2}(x,y,z) = \frac{\partial f^i}{\partial y} \quad (11b)$$

$$J^{i3}(x,y,z) = \frac{\partial f^i}{\partial z} \quad (11c)$$

$\vec{P}$ is then evaluated using the Newton's Method as shown below, and $\overrightarrow{P_k}$ converges to the convergence properties in Table 4 (Equations 12 – 13).

$$\overrightarrow{P_0} = \begin{bmatrix} 0 \\ 0 \\ 0 \end{bmatrix} \quad F_k = \begin{bmatrix} f^1(\overrightarrow{P_k}) \\ f^2(\overrightarrow{P_k}) \\ f^3(\overrightarrow{P_k}) \end{bmatrix} \quad F_0 = \begin{bmatrix} f^1(\overrightarrow{P_0}) \\ f^2(\overrightarrow{P_0}) \\ f^3(\overrightarrow{P_0}) \end{bmatrix}$$

$$J_0 = J(\overrightarrow{P_0}) \qquad J_k = J(\overrightarrow{P_k})$$

$$\Delta\overrightarrow{P_k} = \left(J_k{}^T J_k\right)^{-1} J_k{}^T F_k \quad (12)$$

$$\overrightarrow{P_{k+1}} = \overrightarrow{P_k} - \Delta\overrightarrow{P_k} \quad (13)$$

B. Surface Constraint Derivation

Another assumption that increases the overall accuracy and decreases overall time for a position fix of the scheme is the surface constraint. If the user knows their regional, coarse location and has accurate topographical maps of the area, they can know their altitude on the surface of the planet. This altitude can be used as a constraint in the scheme, allowing for only 2 Doppler measurements to be required instead of 3.

Although the surface constraint decreases the overall time required for a position fix and increases the accuracy, it is important to note that the constraint is optional. However, without the constraint, measurement quantities and window length will have to be extended significantly to reduce 3D position errors to a comparable level.

The surface constraint can be added to LOC by adding the terms from equation 14 to the cost function (Equation 10). *R* is the position of the reference station in cartesian coordinates, and d is the known altitude of the user at point *T*.

$$R = \begin{bmatrix} r_1 \\ r_2 \\ r_3 \end{bmatrix} \qquad d^2 = \left\|\vec{P} + R\right\|^2$$

$$d^2 = (x + r_1)^2 + (y + r_2)^2 + (z + r_3)^2 \quad (14)$$

$$f^i_{surfConst} = f^i + (x + r_1)^2 + (y + r_2)^2 + (z + r_3)^2 - d^2 \quad (15a)$$

$$f^{end}_{surfConst} = (x + r_1)^2 + (y + r_2)^2 + (z + r_3)^2 - d^2 \quad (15a)$$

Likewise, terms can be added to the Jacobian. Equation 16 illustrates the construction of the Jacobian using the surface constraint and when there are 3 time points, that is *i* = 1, 2, and 3. In this case the Jacobian is a *4 x 3* matrix.

Similarly, $\vec{P}$ is then evaluated using the Newton's Method, and $\overrightarrow{P_k}$ converges to the convergence properties in Table 4 (Equations 12 – 13).

$$\overrightarrow{P_0} = \begin{bmatrix} 0 \\ 0 \\ 0 \end{bmatrix} \quad F_k = \begin{bmatrix} f^1_{surfConst}(\overrightarrow{P_k}) \\ f^2_{surfConst}(\overrightarrow{P_k}) \\ f^3_{surfConst}(\overrightarrow{P_k}) \\ f^{end}_{surfConst}(\overrightarrow{P_k}) \end{bmatrix} \quad F_0 = \begin{bmatrix} f^1_{surfConst}(\overrightarrow{P_0}) \\ f^2_{surfConst}(\overrightarrow{P_0}) \\ f^3_{surfConst}(\overrightarrow{P_0}) \\ f^{end}_{surfConst}(\overrightarrow{P_0}) \end{bmatrix}$$

$$J_0 = J(\overrightarrow{P_0}) \qquad J_k = J(\overrightarrow{P_k})$$

C. Single Satellite Multi Measurement Derivation

To acquire multiple measurements from a single satellite, a technique called Single Satellite Multiple Measurement (SSMM) was developed and used in most analysis. With a single satellite, multiple measurements can be taken over the entire pass. Using knowledge of the satellite's and reference station's position and the precise rotation rate of the planet, these measurements can be rotated to the reference frame of the final measurement.

To better visualize the rotations, SSMM was used on the orbit of the Deep Space Habitat (DSH) and a user in Utopia Planitia on Mars.

The first full pass of the DSH occurs at approximately t = 50,000 seconds and ends at approximately t = 75,000 seconds. These were used as the start and end times of the pass and all the measurements were made within this duration. The locations of the DSH, user (Target), and reference station (Base) at each of these times were recorded into Table 4.

Once the final measurement was taken at t = 75,000 seconds, all the previous measurements were rotated to align with the final measurement. This was done by first storing the line of sight (LOS) vector between the reference station and satellite during each measurement. Because of the rotation of Mars, all of the LOS vectors were rotated the same amount that Mars had rotated in the time that had passed since the

respective measurement, and about the same axis and in the same direction as the rotating planet. Once rotated, all of the stored LOS vectors now originate from the same location, the reference station at time tEnd. Now, each of the LOS vectors were treated as separate satellites with their own respective Doppler measurements. The rotated locations were recorded into Table 5, with the rotations performed on these vectors seen in Figure 13.

Although this visualization is for Mars, the same concept can be applied for any other planetary body, including the Moon. For the Marian case, because the DSH is such a large orbit, the wait times between rotations were unfeasibly long. However, because the LRS has a lower orbit, the times between measurements can be from hours to minutes. SSMM was used in all analysis for this paper.

$$J(\vec{P}) = \begin{bmatrix} J^{11}(x,y,z) + 2(x+r_1) & J^{12}(x,y,z) + 2(y+r_2) & J^{13}(x,y,z) + 2(z+r_3) \\ J^{21}(x,y,z) + 2(x+r_1) & J^{22}(x,y,z) + 2(y+r_2) & J^{23}(x,y,z) + 2(z+r_3) \\ J^{31}(x,y,z) + 2(x+r_1) & J^{32}(x,y,z) + 2(y+r_2) & J^{33}(x,y,z) + 2(z+r_3) \\ 2(x+r_1) & 2(y+r_2) & 2(z+r_3) \end{bmatrix} \quad (16)$$

Table 4: DSH, Target, and Base Locations at Each Time in Mars Centered Inertial

Time (s)	Label	DSH Location (Cartesian km)
50,000	tStart	6815.179, 30834.359, 4014.448
62,500	tMid	17807.273, 24211.486, 10489.285
58,000	tMid1	14163.072, 27260.358, 8342.687
66,000	tMid2	20315.958, 21386.269, 11967.014
75,000	tEnd	25168.532, 12651.984, 14825.398
75,000	targetUser	-1401.870, 1853.873, 2466.422
75,000	baseUser	-1409.834, 1847.824, 2466.422

Table 8: DSH Locations Rotated to Align with the Final Measurement

Time (s)	Label	DSH Rotated Location in MCI (Cartesian km)	DSH Rotated Location in MCMF (Aerodetic)
75,000 (was 50,000)	rtStart	-31574.369, 513.343, 4014.447	234.4726° E, 7.2449° N
75,000 (was 62,500)	rtMid	-7490.569, 29106.466, 10489.285	159.8359° E, 19.2392° N
75,000 (was 58,000)	rtMid1	-20390.898, 22976.748, 8342.686	186.9917° E, 15.1935° N
75,000 (was 66,000)	rtMid2	3583.754, 29279.129, 11967.014	138.4257° E, 22.0821° N
75,000	rtEnd	25168.531, 12651.984 14825.398,	77.4861° E, 27.7574° N
75,000	targetUser	-1401.870, 1853.873, 2466.422	180.5° E, 46.7° N
75,000	baseUser	-1409.834, 1847.824, 2466.422	180.7465° E, 46.7° N

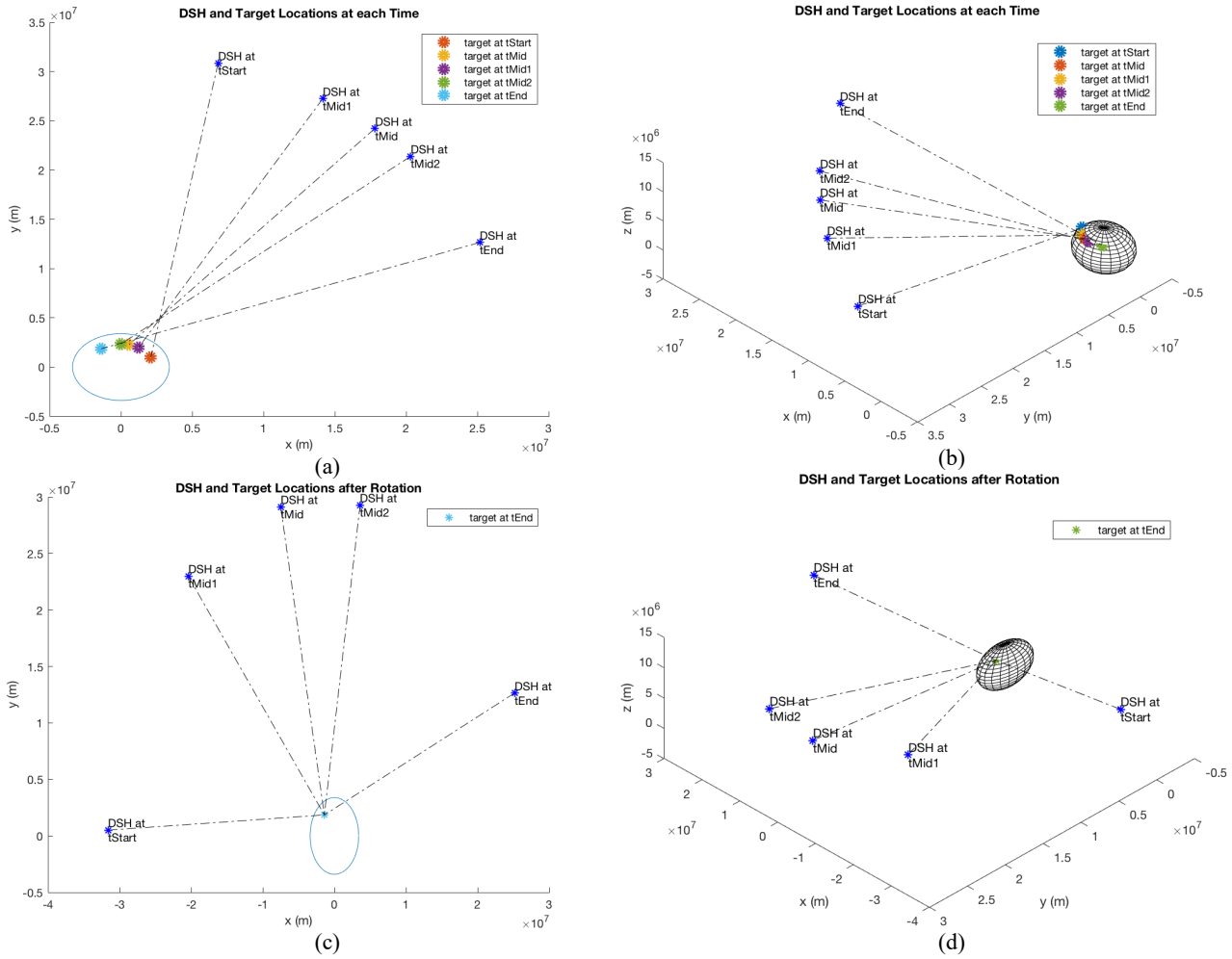

Figure 13: Line of Sight Vectors Between Satellites and Target User Before Rotation in 2D (a) and 3D (b) and After Rotation in 2D (c) and 3D (d)

D. LOC Variable Measurement and Measurement Window Size Analysis

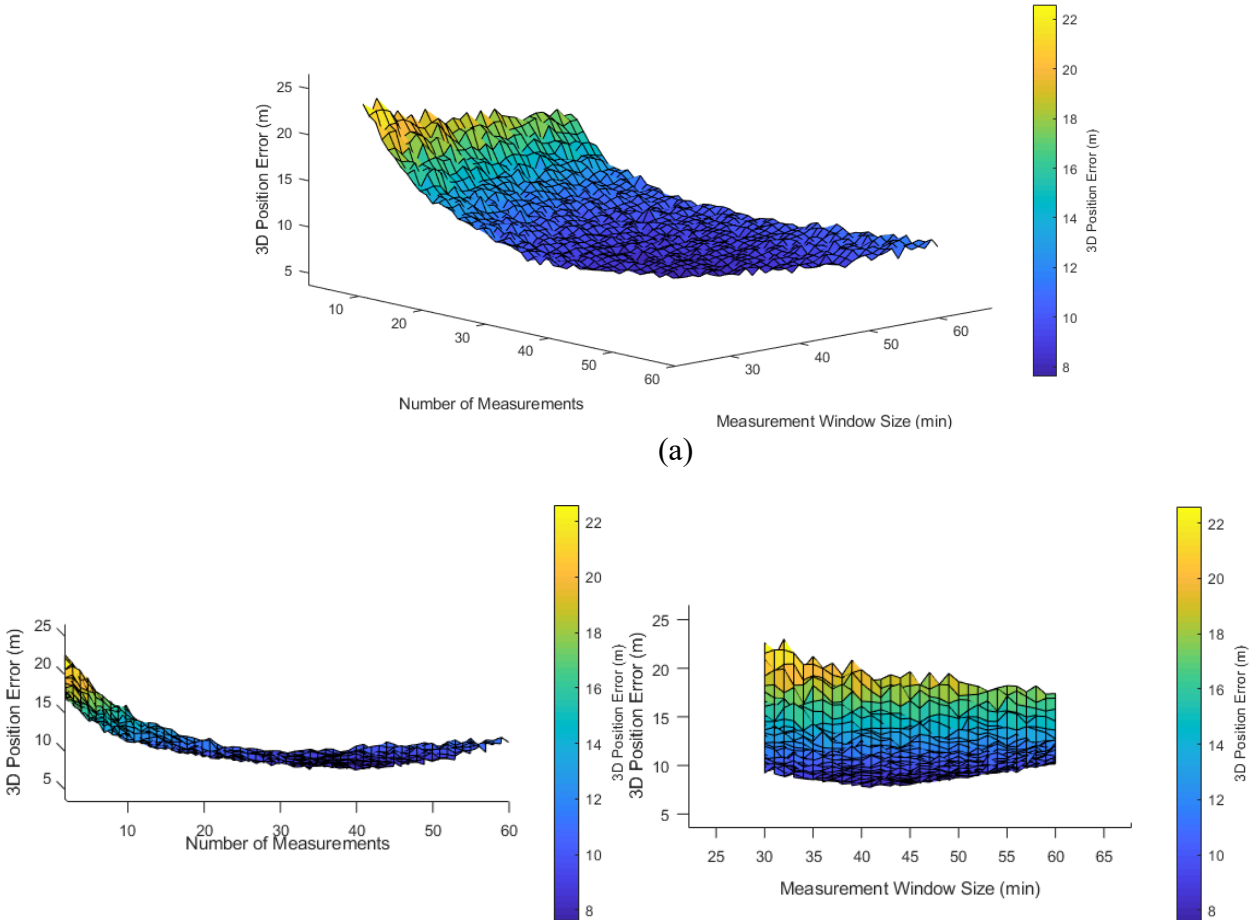

Figure 14: 3D Position Error vs. Measurement Window Size vs. Number of Measurements per Window for LOC at the beginning of the LRS pass. (a) 3D view, (b) side view of relationship with Number of Measurements, (c) front view of relationship with Measurement Window Size

Acknowledgements

The research described in this paper was carried out at the Jet Propulsion Laboratory, California Institute of Technology, under a contract with the National Aeronautics and Space Administration. The research was supported by NASA's Space Communication and Navigation (SCaN) Program.

References

[1] P. Misra and P. Enge, "Global positioning system: Signals, measurements, and performance", Ganga-Jamuna Press, 2001.

[2] Gps.gov. "GPS.gov: Space Segment", https://www.gps.gov/systems/gps/space/ , 2018.

[3] A. Amar and A. J. Weiss, "Localization of Narrowband Radio Emitters Based on Doppler Frequency Shifts", IEEE Transactions on Signal Processing, 2008

[4] B.H. Lee, Y.T. Chan, F. Chan, H-J. Du, F. A. Dilkes, "Doppler Frequency Geolocation of Uncooperative Radars", IEEE Military Communications Conference, 2007

[5] N. H. Nguyen and K. Dogancay. "Algebraic Solution for Stationary Emitter Geolocation by a LEO Satellite Using Doppler Frequency Measurements", IEEE International Conference on Acoustics, Speech, and Signal Processing, 2016

[6] M. Rybak, P. Axelrad, J. Seubert, "Investigation of CSAC Driven One-Way Ranging Performance for CubeSat Navigation", AIAA/USU Conference on Small Satellites, 2018

[7] R.C. Hastrup, D.J. Bell, R.J Cesarone, C.D. Edwards, T.A. Ely, J.R. Guinn, S.N. Rosell, J.M. Srinivasan, S.A. Townes, "Mars Network for Enabling Low-Cost Missions", Acta Astronautica, 2003

[8] F. Wang, X. Zhang, J. Huang, "Error Analysis and Accuracy Assessment of GPS Absolute Velocity Determination without SA", Geo-spatial Information Science, 2008

[9] K. Cheung, W. Jun, G. Lightsey, C. Lee, T. Stevenson, "Single-Satellite Real-Time Relative Localization Using Joint Doppler and Ranging (JDR)," to be submitted to the 70th International Astronautical Congress 2019, Washington, D. C., October 2019.

BIOGRAPHY

Dr. Kar-Ming Cheung *is a Principal Engineer and Technical Group Supervisor in the Communication Architectures and Research Section (332) at JPL. His group supports design and specification of future deep-space and near-Earth communication systems and architectures. Kar-Ming Cheung received NASA's Exceptional Service Medal for his work on Galileo's onboard image compression scheme. Since 1987, he has been with JPL where he is involved in research, development, production, operation, and management of advanced channel coding, source coding, synchronization, image restoration, and communication analysis schemes. He got his B.S.E.E. degree from the University of Michigan, Ann Arbor, in 1984, and his M.S. and Ph.D. degrees from California Institute of Technology in 1985 and 1987, respectively.*

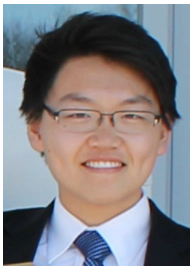

William Jun *is in the process of receiving a B.S. in Aerospace Engineering from the Georgia Institute of Technology in Atlanta, GA. He started his work in navigation architecture during an internship at JPL over the summer of 2018. Over the course of his time at Georgia Tech, he has worked in the Space ms Design Laboratory (SSDL) working on various CubeSat missions as subsystem leads and as the Project Manager of Prox-1. He plans to continue his education with a PhD at Georgia Tech, working under Dr. Glenn Lightsey.*

Professor Charles H. Lee *received his Doctor of Philosophy degree in Applied Mathematics in 1996 from the University of California at Irvine. He then spent three years as a Post-Doctorate Fellow at the Center for Research in Scientific Computation, Raleigh, North Carolina, where he was the recipient of the 1997-1999 National Science Foundation Industrial Post-Doctorate Fellowship. He became an Assistant Professor of Applied Mathematics at the California State University Fullerton in 1999, Associate Professor in 2005, and since 2011 he has been a Full Professor. Dr. Lee has been collaborating with scientists and engineers at NASA Jet Propulsion Laboratory since 2000. His research has been Computational Applied Mathematics with emphases in Aerospace Engineering, Telecommunications, Acoustic, Biomedical Engineering and Bioinformatics. He has published over 65 professionally refereed articles. Dr. Lee received Outstanding Paper Awards from the International Congress on Biological and Medical Engineering in 2002 and the International Conference on Computer Graphics and Digital Image Processing in 2017. Dr. Lee also received NASA's Exceptional Public Achievement Medal in 2018 for the Development of his Innovative Tools to Assess the Communications & Architectures Performance of the Mars Relay Network.*

E. Glenn Lightsey *is a Professor in the Daniel Guggenheim School of Aerospace Engineering at the Georgia Institute of Technology. He is the Director of the Space Systems Design Lab at Georgia Tech. He previously worked at the University of Texas at Austin and NASA's Goddard Space Flight Center. His research program focuses on the technology of satellites, including: guidance, navigation, and control systems; attitude determination and control; formation flying, satellite swarms, and satellite networks; cooperative control; proximity operations and unmanned spacecraft rendezvous; space based Global Positioning System receivers; radionavigation; visual navigation; propulsion; satellite operations; and space systems engineering. At the University of Texas, he founded and directed the Texas Spacecraft Lab which built university satellites. He has written more than 130 technical publications. He is an AIAA Fellow, and he serves as Associate Editor-in-Chief of the Journal of Small Satellites and Associate Editor of the AIAA Journal of Spacecraft and Rockets.*